## Title

THE TRANSIENT AND PERIODIC ILLUMINATION OF A SEMICONDUCTOR-ELECTROLYTE INTERFACE



## Authors

Verbrugge, M.W.
Tobias, C.W.

## Publication Date

1986-08-01

# Lawrence Berkeley Laboratory
UNIVERSITY OF CALIFORNIA

## Materials & Molecular Research Division



Submitted to Journal of the Electrochemical Society

THE TRANSIENT AND PERIODIC ILLUMINATION OF A SEMICONDUCTOR-ELECTROLYTE INTERFACE

M.W. Verbrugge and C.W. Tobias

August 1986



Prepared for the U.S. Department of Energy under Contract DE-AC03-76SF00098

## DISCLAIMER

LBL-21795

# THE TRANSIENT AND PERIODIC ILLUMINATION OF A SEMICONDUCTOR-ELECTROLYTE INTERFACE

Mark W. Verbrugge[1]
and
Charles W. Tobias

Department of Chemical Engineering,
University of California at Berkeley,
and Materials and Molecular Research Division,
Lawrence Berkeley Laboratory
Berkeley, California 94720

August 1986

This work was supported by the Director, Office of Energy Research, Office of Basic Energy Sciences, Materials Sciences Division of the Office of the U.S. Department of Energy, under contract no. DE-AC03-76SF00098.

Keywords: illumination, periodic, photoelectrolysis, semiconductor, transient

[1]Current address: Electrochemistry Department, General Motors Research Laboratories, Warren, Michigan, 48090-9055.

# THE TRANSIENT AND PERIODIC ILLUMINATION OF A SEMICONDUCTOR-ELECTROLYTE INTERFACE

Mark W. Verbrugge[2] and Charles W. Tobias

Department of Chemical Engineering,
University of California at Berkeley,
and Materials and Molecular Research Division,
Lawrence Berkeley Laboratory
Berkeley, California 94720

## ABSTRACT

The analysis of the response of a photoelectrochemical system to a variable light source offers a convenient means for the characterization of a semiconductor-electrolyte interface. We present analytic solutions for the minority-carrier concentrations at the semiconductor surface during pulse, step, sinusoidal, and periodic-square-pulse illumination. The analytic solutions can be used to describe the *low-level-injection* behavior of wide-band-gap semiconductors employed in photoelectrolysis cells and other photoelectrochemical systems.

## Introduction

Since Brattain and Garett's fundamental study of the semiconductor-electrolyte interface (1), there have been large research efforts directed towards understanding and characterizing semiconductor-liquid junctions. Promising photoelectrolysis and solar cell schemes have been advanced based on such an interface (2). Bard (3) and Heller (4) have recently reviewed efficient photoelectrochemical (PEC) systems, elucidating problems and progress.

A useful technique in the characterization of PEC cells is to analyze the system's response to a varying light source (5,6,7). This is analogous to varying the current or potential (chronopotentiometry or chronoamperometry, respectively) in the study of traditional, non-photoactive electrochemical systems. In this work, we present analytic solutions for minority-carrier transport equations that allow for the description of a PEC cell subject to pulse, step, sinusoidal, and periodic square-pulse illumination. This treatment is an extension of existing steady-state

[2]Current address: Electrochemistry Department, General Motors Research Laboratories, Warren, Michigan, 48090-9055.

models by Gartner (8) and Dewald (9). These models have been shown by a number of authors to predict accurately the behavior of wide-band-gap PEC systems (10,11,12,13,14).

The response of a photoactive system to a varying light intensity has been the subject of many studies. van Roosbroeck examined injected current-carrier transport in a semiconductor as a means to determine carrier lifetimes and surface-recombination velocities (15). Following van Roosbroeck's study, numerous researchers have addressed the response of PEC systems under varying illumination intensities (*e.g.* 16,17,18,19,20). In addition, Laser and Bard implemented a more general digital-simulation model to study transient charge injection in a PEC cell (21).

The major emphasis of this treatment deals with the solution to the equations describing minority-carrier transport in the semiconductor; this is because semiconductor-electrolyte interfaces are often analogous to *Schottky barriers* in metal-semiconductor contacts, and the electrolyte-species transport usually plays a minor role in the determining the PEC system behavior (1,22). For the description of many PEC systems, it is necessary to incorporate kinetic resistances at the interface (23,24). The next section of this work addresses the proper use of a semiconductor-electrode kinetic expression. Following this, we present solutions for the minority-carrier transport equations.

## The Interfacial Kinetic Expression

A number of treatments for the analysis of semiconductor-electrolyte interfaces indicate that a Butler-Volmer type equation is the best expression available to describe the current-potential relationship (*e.g.* 2,11,13,25). In the following, we shall demonstrate the use of a Butler-Volmer equation for the description of the current-potential relationship of a PEC cell. Particular attention must be paid to the metal-semiconductor space-charge region as well as the semiconductor-electrolyte region of charge separation.

In the following discussion, we treat the reaction of semiconductor electrons with species in the electrolyte. An analogous treatment can be used to describe reactions with semiconductor holes. We shall not address activity coefficient corrections in this work. For the electrochemical reaction

$$\mathrm{O} + n\mathrm{e}^- \rightleftharpoons \mathrm{R} \tag{1}$$

the current-potential relationship is

$$\frac{i}{nF} = k_a \exp[(1-\beta)nfV]\frac{c_{\mathrm{R}}}{\rho_o} - k_c \exp(-\beta nfV)\frac{c_{\mathrm{O}}}{\rho_o}c_{e^-} , \tag{2}$$

where surface concentrations are used, $f = F/(RT)$, and

$$V = E + \left[U^{\theta}_{ref} - \frac{1}{n_{ref} f} \sum_i s_{i,ref} \ln\left(\frac{c_{i,ref}}{\rho_o}\right)\right] - \Delta\Phi_{IR} - \Delta\Phi_{SE} - \Delta\Phi_{MS} \,. \tag{3}$$

The potential of a platinum wire, intimately contacted to the semiconductor, with respect to a reference electrode is the measured cell potential $E$. The bracketed term in Eq. 3 represents a Nernst expression for the reference electrode, denoted henceforth as $U^{eq}_{ref}$. The cell ohmic-potential drop is represented by $\Delta\Phi_{IR}$. The potential differences across the space-charge regions in the semiconductor near the metal-semiconductor and semiconductor-electrolyte interfaces are denoted by $\Delta\Phi_{MS}$ and $\Delta\Phi_{SE}$, respectively. The symbol $\Delta$ preceding $\Phi_{MS}$ and $\Phi_{SE}$ refers to spatial differences; hence $\Delta\Phi_{MS}$ is the value of the electric potential at the metal side of the metal-semiconductor space-charge region less the value of the electric potential at the semiconductor side of the space-charge region. Similarly, $\Delta\Phi_{SE}$ is the value of the electric potential at the semiconductor side of the semiconductor-electrolyte space-charge region less the value of the electric potential at the electrolyte side of the space-charge region. Therefore, the potential difference between a platinum wire contacted to the semiconductor and a normal hydrogen electrode (NHE), corrected for ohmic drop and potential differences across the space-charge regions, is represented by $V$. The potential difference across the diffuse portion of the double layer in the electrolyte is usually very small and is neglected in this work (2).

At equilibrium, $i = 0$, and Eq. 2 reduces to

$$V^{eq} = \frac{1}{nf} \ln \frac{k_c}{k_a} + \frac{1}{nf} \ln \frac{c_{\mathrm{O}} c^n_{e^-}}{c_{\mathrm{R}}} \tag{4}$$

or

$$FV^{eq} = \frac{1}{n}(\mu^{\theta}_{\mathrm{O}} + n\mu^{o,\mathrm{Pt}}_{e^-} - \mu^{\theta}_{\mathrm{R}}) + \frac{RT}{n} \ln \frac{c_{\mathrm{O}} c^n_{e^-}}{c_{\mathrm{R}}} \,. \tag{5}$$

In this work, we make use of the following dilute-solution expression for the electrochemical potential (26,27)

$$\mu_i = \mu^{ref}_i + RT \ln c_i + z_i F \Phi. \tag{6}$$

The first two terms on the right side of Eq. 6 represent purely chemical contributions. The superscript $\theta$ in Eq. 5 denotes a reference state of infinite dilution in an aqueous phase. Since the rate constants are related to the NHE, the superscript $o,\mathrm{Pt}$ is required to denote the standard state electrochemical potential of the electrons in platinum, the electrode material used in the NHE. Equation 5 can

be combined with Eq. 3 to yield the measured, equilibrium cell voltage

$$FE^{eq} = \frac{1}{n}(\mu_{O}^{\theta} + n\mu_{e^-}^{o,s} - \mu_{R}^{\theta}) + \frac{RT}{n}\ln\frac{c_O}{c_R} + \mu_{e^-}^{o,Pt} - \mu_{e^-}^{o,s} + RT\ln c_{e^-} + F(\Delta\Phi_{MS} + \Delta\Phi_{SE} - U_{ref}^{eq}), \quad (7)$$

where $\mu_{e^-}^{o,s}$ represents the standard-state electrochemical potential of electrons in the semiconductor.

In dilute solutions that are under equilibrium conditions, a Boltzmann expression can be used to relate ionic concentrations to potential differences within a conducting phase (28):

$$c_{e^-} = c_{e^-}^{b,s}\exp(-f\Delta\Phi_{SE}) \quad (8)$$

$$c_{e^-}^{b,s} = c_{e^-}^{Pt}\exp(-f\Delta\Phi_{MS}) \quad (9)$$

where the superscript $b,s$ denotes the bulk semiconductor. The cell voltage can then be expressed by inserting Eqs. 8 and 9 into Eq. 7:

$$FE^{eq} = (\mu_{e^-}^{o,Pt} + RT\ln c_{e^-}^{Pt}) - (\mu_{e^-}^{o,s} + RT\ln c_{e^-}^{b,s}) + \frac{1}{n}(\mu_{O}^{\theta} + n\mu_{e^-}^{o,s} - \mu_{R}^{\theta}) + \frac{RT}{n}\ln\frac{c_O c_{e^-}^{b,s}}{c_R} + (\frac{1}{2}\mu_{H_2}^{\theta} - \mu_{H^+}^{\theta} - \mu_{e^-}^{o,Pt}) + RT\ln\frac{\sqrt{c_{H_2}}}{c_{H^+}c_{e^-}^{o,Pt}} \quad (10)$$

The first two terms on the right side of Eq. 10 represents the potential difference between the platinum contact and the bulk semiconductor. The third and fourth terms represent the potential difference across the semiconductor-electrolyte interface. The last two terms indicate that a hydrogen reference electrode has been assumed. This is the same expression that is obtained if the cell potential is expressed by summing the potential differences between the various phases at equilibrium (29). Equation 10 can be further simplified by canceling the semiconductor terms (denoted with superscript $s$) and platinum terms (denoted with superscript Pt). As is expected, the open-circuit cell potential is independent of the semiconductor phase.

It is important to note that the potential difference across the space-charge region near the metal-semiconductor contact $\Delta\Phi_{MS}$ had to be included in order to develop rigorously the cell-potential expression. This term is often neglected in semiconductor-electrode analyses. $\Delta\Phi_{MS}$ is also a function of cell polarization; for a uniformly doped semiconductor, a Schottky-barrier analysis may suffice. It is also possible to alter the dopant concentration to minimize $\Delta\Phi_{MS}$ (30). In general, the theory is well developed for metal-semiconductor contacts, and we will only address the semiconductor-electrolyte contact.

## Evaluation of the Minority-Carrier Concentration

Although the treatment we present in this section for the solution to the minority-carrier transport is approximate, its steady-state counterpart has proved to be a valuable tool for the description of many PEC systems. More complete discussions of the full equations governing electron, hole, and ionic transport have been presented by Orazem and Newman (25,31). In order to develop the cell current-potential relationship, the relation between the cell current and $\Delta\Phi_{MS}$ is required, and Gauss' law must be incorporated to solve for $\Delta\Phi_{SE}$ and for the surface overpotential associated with the charge-transfer reaction across the Helmholtz layer. For extrinsic semiconductors, usually the *depletion approximation* can be used to simplify the evaluation of $\Delta\Phi_{SE}$, resulting in a parabolic potential distribution across the space-charge region. (*cf.* ref. 2, Eq. 23) The potential drop across the Helmholtz layer is usually assumed to vary linearly. (*cf.* ref. 25, Eqs. 29 and 30)

The three regions of interest in this analysis, the electrolyte, the semiconductor space-charge layer, and the neutral semiconductor, are shown in Fig. 1. The semiconductor is represented by a space-charge region for $0 < x < w$ and an electrically neutral region for $x > w$.

The space-charge layer is modeled as an equilibrated region of minority carriers (electrons in a p-semiconductor, holes in an n-semiconductor). The equilibrium assumption is usually justified because small concentration and potential variations across the thin space-charge region give rise to large gradients in concentration and potential, and to large, opposing diffusion and migration fluxes. A minority-carrier flux balance on the region yields

$$-\frac{i}{z_i F} + \int_0^w I(t) a e^{-ax} dx = N|_{x=w} + v_s(c^w - c^b). \qquad (11)$$

The first term is related to the flux of minority carriers into the region by electrochemical reaction. For holes, $z_i = 1$ and for electrons, $z_i = -1$. Anodic currents are taken as positive in this work. The second term represents generation by illumination. The flux of minority carriers out of the region, $N|_{x=w}$, is obtained by solving the continuity equation for the minority carrier in the semiconductor. The last term in Eq. 11 represents a very approximate treatment for surface recombination. The surface-recombination term is similar to a Shockley, Hall, Read surface-recombination model (32,33) if the energies of the trap sites are located near midgap, the hole and electron *capture cross sections* are identical, and the charge carriers are at low concentration.

In Gartner's treatment surface recombination is neglected, and the minority-carrier concentration is set to zero at $x = w$. The Gartner model begins to fail for systems with negligible space-charge widths, or small potential drops across the

space-charge region. Including the recombination term and a non-zero minority-carrier concentration at $x = w$ represent additions to the Gartner model that appear in Dewald's work and improve the analysis of PEC cells (13).

The dilute-solution, one-dimensional equation of continuity for the description of the minority-carrier transport within the bulk semiconductor is

$$\frac{\partial c}{\partial t} = D\frac{\partial^2 c}{\partial x^2} - \frac{c - c^b}{\tau} + I(t)a\mathrm{e}^{-ax}. \tag{12}$$

Migration terms are not included in the continuity expression since the majority-carrier concentration is assumed large and invariant, thus acting as a supporting electrolyte and reducing the effect of the electric field on minority-carrier transport. This is usually a good assumption for extrinsic semiconductors. The bulk-recombination model, which makes use of the *carrier lifetime* $\tau$ is analogous to the surface-recombination model used in Eq. 11 and embodies the same assumptions. The exclusion of the electric field effects and the use of a simple recombination model are more valid approximations for *low-level-injection* situations. In general, the treatment we present is analogous to the *ideal-diode analysis*, in which both of these assumptions are made (34,35,36).

The boundary conditions and initial condition are:

$$c(t,\infty) = c^b \tag{13}$$

$$c(t,w) = c^w \tag{14}$$

$$c(0,x) = c^{init}(x) \tag{15}$$

The first boundary condition states that the minority-carrier concentration reaches its bulk value at large distances from the interface. This boundary condition is valid for semiconductor thicknesses substantially greater $\sqrt{\tau D}$, the characteristic length for this transport problem, also denoted by $L$, the *diffusion length.* The second boundary condition sets the concentration at $x = w$. In the last condition, the initial concentration profile is set equal to the steady-state value for constant illumination. The full steady-state solution, with constant illumination intensity $I$, is:

$$c(x) = c^b - \frac{\frac{i}{z_i F} - I\left(1 - \frac{\mathrm{e}^{-aw}}{aL+1}\right)}{v_s + \frac{L}{\tau}}\mathrm{e}^{-\frac{x-w}{L}} - \frac{Ia\tau\mathrm{e}^{-wa}}{(aL)^2 - 1}\left[\mathrm{e}^{-a(x-w)} - \mathrm{e}^{-\frac{x-w}{L}}\right] \tag{16}$$

At zero current ($i = 0$) and no illumination ($I = 0$), the minority-carrier concentration is equal to its bulk value for all $x \geq w$. For the problems solved in this work, the interface was initially not illuminated.

The solution to the system of equations 12 – 15 can be combined with Eq. 11 to yield $c^w$. If the *quasi-equilibrium assumption* is invoked, the charge carriers are assumed to be in translational equilibrium across the space-charge region (9), and the surface concentration can be related to $c^w$ by a Boltzmann factor, $c^{surf} = c^w \exp(z_i f \Delta\Phi_{SE})$.

Equations 12 – 15 can be non-dimensionalized with the following definitions:

$$\varsigma = \frac{x - w}{L} \tag{17}$$

$$\theta = \frac{t}{\tau} \tag{18}$$

$$\Theta = \frac{c - c^b}{c^b} \tag{19}$$

$$\alpha = aL \tag{20}$$

$$\lambda = -\frac{i}{z_i F (v_s + \frac{D}{L}) c^b} \tag{21}$$

$$\phi = \frac{I(t) a r e^{-aw}}{c^b} \tag{22}$$

These definitions can be used to restate the problem:

$$\frac{\partial \Theta}{\partial \theta} = \frac{\partial^2 \Theta}{\partial \varsigma^2} - \Theta + \phi(\theta) e^{-\alpha \varsigma} \tag{23}$$

$$\Theta(\theta, \infty) = 0 \tag{24}$$

$$\Theta(\theta, 0) = \Theta^w \tag{25}$$

$$\Theta(0, \varsigma) = \lambda e^{-\varsigma} \tag{26}$$

Equation 23 is a linear, partial-differential equation with constant coefficients. The Laplace transform technique can be used to reduce Eq. 23 to an ordinary differential equation:

$$\frac{d^2 \overline{\Theta}}{d\varsigma^2} - \overline{\Theta}(s + 1) = -\lambda e^{-\varsigma} - \phi(s) e^{-\alpha \varsigma}, \tag{27}$$

where $s$ is the Laplace transform variable and an overbar indicates a transformed variable. The transformed boundary conditions are:

$$\overline{\Theta}(\infty) = 0 \tag{28}$$

$$\overline{\Theta}(0) = \frac{\Theta^w}{s} \tag{29}$$

The solution to the system of equations 27 – 29 is

$$\overline{\Theta} = \left[ \frac{(\Theta^w - \lambda)}{s} - \frac{\phi(s)}{s + 1 - \alpha^2} \right] e^{-\sqrt{s+1}\varsigma} + \frac{\lambda}{s} e^{-\varsigma} + \frac{\phi(s) e^{-\alpha \varsigma}}{s + 1 - \alpha^2}. \tag{30}$$

The flux of the minority carrier at $x = w$, in Laplace space, is

$$\overline{N}\Big|_{x=w} = -c^b \frac{D}{L} \frac{d\overline{\Theta}}{d\zeta}\Big|_{\zeta=0} , \tag{31}$$

where

$$\frac{d\overline{\Theta}}{d\zeta}\Big|_{\zeta=0} = -\left[\frac{(\Theta^w - \lambda)}{s} - \frac{\phi(s)}{s+1-\alpha^2}\right]\sqrt{s+1} - \frac{\lambda}{s} - \frac{\phi(s)\alpha}{s+1-\alpha^2} . \tag{32}$$

The inversion of Eq. 31 yields $N|_{x=w}$, which can be used in Eq. 11 to obtain the minority-carrier concentration $c^w$, $\Theta^w$ in dimensionless terms. Combining the inverted expression for Eq. 31 with Eq. 11 yields

$$\overline{\Theta}^w - \sigma_1 \frac{d\overline{\Theta}}{d\zeta}\Big|_{\zeta=0} = \sigma_2, \tag{33}$$

where $\sigma_1$ and $\sigma_2$ are dimensionless groups introduced for convenience:

$$\sigma_1 = \frac{D}{Lv_s} \tag{34}$$

$$\sigma_2(t) = -\frac{1}{v_s c^b}\left[\frac{i}{z_i F} + I(t)(e^{-\alpha w} - 1)\right] \tag{35}$$

The next portion of this work addresses the evaluation of $\frac{d\Theta}{d\zeta}\Big|_{\zeta=0}$ and $\Theta^w$.

*Light impulse* - The light-flux function is shown in Fig. 2. In the limit of vanishingly small pulse width $\Delta t$, the Laplace transform of the light impulse with area $I_o$ is $\phi(s) = \phi_o$ in dimensionless form (ref. 37, p. 65). Substituting this value of $\phi(s)$ into Eq. 32, and inverting yields

$$\frac{d\Theta}{d\zeta}\Big|_{\zeta=0} = (\lambda - \Theta^w)e^{-\theta}\left[\frac{1}{\sqrt{\pi\theta}} + e^{\theta}\mathrm{erf}(\sqrt{\theta})\right] + \tag{36}$$
$$\phi_o e^{-\theta}\left[\frac{1}{\sqrt{\pi\theta}} + \alpha e^{\alpha^2\theta}\mathrm{erf}(\alpha\sqrt{\theta})\right] - \lambda - \phi_o \alpha e^{(\alpha^2-1)\theta} .$$

The inversions required to obtain Eq. 36 can be found in most Laplace transform tables (*e.g.* 38,39,40) after the translation properties of Laplace transform (ref. 37, pp. 60-61) are used on the function $\frac{d\overline{\Theta}}{d\zeta}\Big|_{\zeta=0}$.

The concentration $\Theta^w$ can be found by substituting Eq. 36 into Eq. 33:

$$\Theta^w = \frac{1}{1 + \sigma_1 e^{-\theta}\left[\frac{1}{\sqrt{\pi\theta}} + e^{\theta}\mathrm{erf}(\sqrt{\theta})\right]}\left(\sigma_2 + \sigma_1\left\{\lambda e^{-\theta}\left[\frac{1}{\sqrt{\pi\theta}} + \right.\right.\right. \tag{37}$$
$$\left.\left.\left. e^{\theta}\mathrm{erf}(\sqrt{\theta}) - e^{\theta}\right] + \phi_o e^{-\theta}\left[\frac{1}{\sqrt{\pi\theta}} + \alpha e^{\alpha^2\theta}\left(\mathrm{erf}(\alpha\sqrt{\theta}) - 1\right)\right]\right\}\right)$$

For long times, $\Theta^w = \sigma_2/(1+\sigma_1)$, or

$$\Theta^w = -\frac{i}{z_i F c^b \left(v_s + \frac{D}{L}\right)} \tag{38}$$

which is the expected result in view of Eq. 16.

*Light step* - The light-step function is shown in Fig. 3. For this step function, $\phi(s) = \phi_o/s$. Substituting this value of $\phi(s)$ into Eq. 32, we obtain the following expression for $\left.\frac{d\overline{\Theta}}{d\varsigma}\right|_{\varsigma=0}$:

$$\left.\frac{d\overline{\Theta}}{d\varsigma}\right|_{\varsigma=0} = -\left[\frac{\Theta^w - \lambda}{s} - \frac{\phi_o}{s(s+1-\alpha^2)}\right]\sqrt{s+1} - \frac{\lambda}{s} - \frac{\phi_o \alpha}{s(s+1-\alpha^2)} \tag{39}$$

The inversion of $\sqrt{s+1}/[s(s+1-\alpha^2)]$ is presented in the Appendix. The complete inversion of Eq. 39 gives

$$\begin{aligned}\left.\frac{d\Theta}{d\varsigma}\right|_{\varsigma=0} = {} & (\lambda - \Theta^w)e^{-\theta}\left[\frac{1}{\sqrt{\pi\theta}} + e^{\theta}\mathrm{erf}(\sqrt{\theta})\right] + \\ & \frac{\phi_o}{\alpha^2-1}\left[\alpha\mathrm{erf}(\alpha\sqrt{\theta})e^{(\alpha^2-1)\theta} - \mathrm{erf}(\sqrt{\theta})\right] - \\ & \lambda - \frac{\phi_o\alpha}{\alpha^2-1}\left[e^{(\alpha^2-1)\theta} - 1\right].\end{aligned} \tag{40}$$

Combining Eqs. 33 and 40 yields

$$\begin{aligned}\Theta^w = {} & \frac{1}{1+\sigma_1 e^{-\theta}\left[\frac{1}{\sqrt{\pi\theta}} + e^{\theta}\mathrm{erf}(\sqrt{\theta})\right]} \times \\ & \left(\sigma_2 + \sigma_1\left\{\lambda e^{-\theta}\left[\frac{1}{\sqrt{\pi\theta}} + e^{\theta}\mathrm{erf}(\sqrt{\theta}) - e^{\theta}\right] + \right.\right. \\ & \left.\left.\frac{\phi_o}{\alpha^2-1}\left[\alpha\mathrm{erf}(\alpha\sqrt{\theta})e^{(\alpha^2-1)\theta} - \mathrm{erf}(\sqrt{\theta}) + \alpha\left(1 - e^{(\alpha^2-1)\theta}\right)\right]\right\}\right).\end{aligned} \tag{41}$$

For long times,

$$\Theta^w = \frac{\sigma_2 + \frac{\phi_o}{\alpha+1}\sigma_1}{1+\sigma_1}, \tag{42}$$

or

$$\Theta^w = -\frac{\frac{i}{z_i F} - I_o\left[1 - \frac{e^{-w\alpha}}{1+\alpha L}\right]}{c^b\left(v_s + \frac{D}{L}\right)}. \tag{43}$$

This agrees with Eq. 16 evaluated at $x = w$.

*Periodic square-pulse illumination* - The light source is depicted in Fig. 4. The light source can be expressed by a Fourier series (41)

$$I(t) = \frac{J_o + I_o}{2} + (J_o - I_o)\frac{2}{\pi}\sum_{i=1,3,5,\ldots}^{\infty}\frac{1}{i}\sin\left(\frac{i\pi\theta}{\theta_T}\right), \tag{44}$$

where the dimensionless half-cycle period is $\theta_T = T/\tau$. The treatment for a sinusoidal light source is identical to this problem, as can be seen by inspection of Eq. 44. Inverting and substituting Eq. 44 into Eq. 32 yields:

$$\left.\frac{d\overline{\Theta}}{d\varsigma}\right|_{\varsigma=0} = \left(\left.\frac{d\overline{\Theta}}{d\varsigma}\right|_{\varsigma=0}\right)_{step} - \Psi_i\left[\frac{\alpha}{(s^2+\gamma_i^2)(s+1-\alpha^2)} - \frac{\sqrt{s+1}}{(s^2+\gamma_i^2)(s+1-\alpha^2)}\right], \tag{45}$$

where $\gamma_i = i\pi/\theta_T$ and $\Psi_i$ is the operator

$$\Psi_i = \frac{2(J_o - I_o)a\tau e^{-wa}}{c^b\theta_T}\sum_{i=1,3,5,\ldots}^{\infty}. \tag{46}$$

The term $\left(\left.\frac{d\overline{\Theta}}{d\varsigma}\right|_{\varsigma=0}\right)_{step}$ represents a light step to $(I_o+J_o)/2$, which can be evaluated with Eq. 39. The inversion of Eq. 45 is outlined in the Appendix. The result is

$$\left.\frac{d\Theta}{d\varsigma}\right|_{\varsigma=0} = \left(\left.\frac{d\Theta}{d\varsigma}\right|_{\varsigma=0}\right)_{step} - \Psi_i\left(\left[\frac{\Xi_1}{\gamma_i}\cos(\gamma_i\theta) - \frac{\Xi_2}{\gamma_i}\sin(\gamma_i\theta)\right] + \frac{\alpha}{(\alpha^2-1)^2+\gamma_i^2}\left\{\frac{1-\alpha^2}{\gamma_i}\sin(\gamma_i\theta) - \cos(\gamma_i\theta) + e^{(\alpha^2-1)\theta} - \operatorname{erf}(\alpha\sqrt{\theta})e^{(\alpha^2-1)\theta} + \alpha\left[\Xi_1\sin(\gamma_i\theta) + \Xi_2\cos(\gamma_i\theta)\right] + \frac{\alpha(1-\alpha^2)}{\gamma_i}\left[\Xi_1\cos(\gamma_i\theta) - \Xi_2\sin(\gamma_i\theta)\right]\right\}\right). \tag{47}$$

The step solution $\left(\left.\frac{d\Theta}{d\varsigma}\right|_{\varsigma=0}\right)_{step}$ is expressed in Eq. 40, with $\phi_o = (I_o + J_o)a\tau e^{-wa}/(2c^b)$. The functions $\Xi_1$ and $\Xi_2$ are:

$$\Xi_1 = \frac{1}{\sqrt{\pi}}\sum_{j=0}^{\infty}\sum_{k=0}^{\infty}\frac{(-1)^{j+k}\gamma_i^{2k+1}\theta^{j+2k+3/2}}{j!(2k+1)!(j+2k+3/2)} \tag{48}$$

$$\Xi_2 = \frac{1}{\sqrt{\pi}}\sum_{j=0}^{\infty}\sum_{k=0}^{\infty}\frac{(-1)^{j+k}\gamma_i^{2k}\theta^{j+2k+1/2}}{j!(2k)!(j+2k+1/2)} \tag{49}$$

For long times, the exponential terms in Eq. 47 vanish, and the functions $\Xi_1$ and $\Xi_2$ reach limiting values (see Appendix):

$$\Xi_1 = \left[\frac{\sqrt{1+\gamma_i^2}-1}{2(\gamma_i^2+1)}\right]^{1/2} \qquad (\theta \to \infty) \tag{50}$$

$$\Xi_2 = \left[\frac{\sqrt{1+\gamma_i^2}+1}{2(\gamma_i^2+1)}\right]^{1/2} \qquad (\theta \to \infty) \tag{51}$$

Inserting Eq. 47 into Eq. 33 yields $\Theta^w$:

$$\Theta^w - \Theta^{w,step} = \tag{52}$$

$$\frac{-\sigma_1\Psi_i}{1+\sigma_1 e^{-\theta}\left[\frac{1}{\sqrt{\pi\theta}}+e^{\theta}\mathrm{erf}(\sqrt{\theta})\right]}\left(\left[\frac{\Xi_1}{\gamma_i}\cos(\gamma_i\theta)-\frac{\Xi_2}{\gamma_i}\sin(\gamma_i\theta)\right]+\right.$$
$$\frac{\alpha}{(\alpha^2-1)^2+\gamma_i^2}\left\{\frac{1-\alpha^2}{\gamma_i}\sin(\gamma_i\theta)-\cos(\gamma_i\theta)+e^{(\alpha^2-1)\theta}-\mathrm{erf}(\alpha\sqrt{\theta})e^{(\alpha^2-1)\theta}+\right.$$
$$\left.\left.\frac{\alpha(1-\alpha^2)}{\gamma_i}\left[\Xi_1\cos(\gamma_i\theta)-\Xi_2\sin(\gamma_i\theta)\right]+\alpha\left[\Xi_1\sin(\gamma_i\theta)+\Xi_2\cos(\gamma_i\theta)\right]\right\}\right)$$

where $\Theta^{w,step}$ is represented by the mathematical expression of Eq. 41. It should be noted, however, that $\sigma_2$ is a function of time. Hence, $\Theta^{w,step}$, which contains $\sigma_2(\theta)$, will vary since $I(t)$ changes periodically from $I_o$ to $J_o$. For long times, $\Theta^{w,step} = \frac{\sigma_2(\theta)+\frac{\phi_o}{\alpha+1}\sigma_1}{1+\sigma_1}$, and the exponential terms in Eq. 52 vanish, leaving the following long-time solution:

$$\Theta^w = \frac{\sigma_2(\theta)+\frac{\phi_o}{\alpha+1}}{1+\sigma_1}-\frac{\sigma_1\Psi_i}{1+\sigma_1}\left(\left[\frac{\Xi_1}{\gamma_i}\cos(\gamma_i\theta)-\frac{\Xi_2}{\gamma_i}\sin(\gamma_i\theta)\right]+\right. \tag{53}$$
$$\frac{\alpha}{(\alpha^2-1)^2+\gamma_i^2}\left\{\frac{1-\alpha^2}{\gamma_i}\sin(\gamma_i\theta)-\cos(\gamma_i\theta)+\right.$$
$$\alpha\left[\Xi_1\sin(\gamma_i\theta)+\Xi_2\cos(\gamma_i\theta)\right]+$$
$$\left.\left.\frac{\alpha(1-\alpha^2)}{\gamma_i}\left[\Xi_1\cos(\gamma_i\theta)-\Xi_2\sin(\gamma_i\theta)\right]\right\}\right)$$

To implement Eq. 53, the long-time representations for $\Xi_1$ and $\Xi_2$, which are given in Eqs. 50 and 51, should be used. The function $\Theta^w$ attains a uniform and sustained periodic state. Since the system reaches a periodic state, and the mathematical description is analytic and straightforward, this technique is promising as a convenient analytical tool.

Table 1. Input values for Figs. 5, 6, 7, and 8.

| Quantity | Value | Units | |
|---|---|---|---|
| $a$ | 1667 | 1/cm | † |
| $c^b$ | $1.660 \times 10^{-19}$ | $mol/cm^3$ | |
| $D$ | 0.2567 | $cm^2/s$ | † |
| $I_o$ | $6.392 \times 10^{-16}$ | $mol/cm^2 - s$ | ‡ |
| $J_o$ | $6.392 \times 10^{-16}$ | $mol/cm^2 - s$ | |
| $\tau$ | $9.739 \times 10^{-9}$ | s | † |
| $v_s$ | 2567 | cm/s | |

† These values were obtained from the work of Butler (11) and are characteristic of $WO_3$. All other values were estimated.
‡ For the sinusoidal light-flux function, $I_o = 0$.

## Results

In this section, we examine the behavior of the derived equations. Since the model work is most applicable to wide-band-gap semiconductors, available values for the physicochemical parameters characteristic of $WO_3$, a wide-band-gap semiconductor studied by Butler (11), were employed in our analysis. The values of the parameters required for the analysis are presented in Table 1.

The purpose of this section is to illustrate the behavior of the solutions to the transport equations. For this reason, we investigate cases with minimal resistance to charge-transfer reactions and negligible ohmic loss. Under these conditions, a convenient reference potential is the flat-band potential, $V_{FB}$. The flat-band potential corresponds to the potential that the working electrode must be maintained for there to be no charge separation at the semiconductor-electrolyte interface. At this potential, the width of the space-charge region $w$ is zero.

A further simplification that we use is the depletion approximation, which was discussed briefly at the beginning of the previous section. With this approximation,

$$V - V_{FB} = \frac{1}{z_o f} \frac{w^2}{\lambda_D^2} , \tag{54}$$

where $\lambda_D$ is a Debye length

$$\lambda_D = \left( \frac{2\epsilon_s RT}{F^2 z_o^2 N_o} \right)^{1/2} . \tag{55}$$

To examine the behavior of the minority-carrier transport solutions, we present results for the case of $c^w = 0$. For example, under the stated conditions, the

steady-state current density can be expressed as (*cf.* Eq. 16)

$$\frac{i}{i_{LIM}} = 1 + \frac{I}{(v_s + \frac{D}{L})c^b}\left\{1 - \frac{\exp\left[-a\lambda_D\sqrt{z_o f(V - V_{FB})}\right]}{(aL+1)}\right\}, \qquad (56)$$

where $i_{LIM}$ is the steady-state limiting-current density of the minority carrier when the semiconductor is not illuminated:

$$i_{LIM} = z_i F\left(v_s + \frac{D}{L}\right)c^b \qquad (57)$$

Expressions similar in form, though algebraically more complex, to Eq. 56 can be written for pulse, step, sinusoidal, and periodic-square-pulse illumination. As was done for the development of Eq. 56, Eq. 54 is substituted into the relevant transport solution (Eq. 37, 41, or 52), and $c^w$ is set equal to zero.

The results for light-impulse illumination are shown in Fig. 5. The initially large current density decays to the value $i_{LIM}$ given by Eq. 57. The light-step results of Fig. 6 also show that a steady-state is reached after $t/\tau = 5$. In the light-step case, the steady-state value of $i/i_{LIM}$ corresponds to that of Eq. 56.

The current-time behavior of a semiconductor-electrolyte interface under sinusoidal illumination, after the system has achieved a uniform and sustained periodic state, is shown in Fig. 7. For this case, $V - V_{FB}$ was set equal to a small value, which corresponds to a narrow space-charge region (*cf.* Eq. 54). Consequently, most of the light is absorbed in the neutral semiconductor region described by Eq. 53, the long-time solution. It can be seen that for large values of $T_c/\tau$, reflecting a large cycle period to carrier lifetime, a pseudosteady-state condition results; for the case of $T_c/\tau = 100$, $i/i_{LIM}$ could have been obtained by simply inserting the time-dependent light flux, $I(t)$, into Eq. 56. Conversely, for the case of small $T_c/\tau$, illustrated by the solid line in Fig. 5, only small-amplitude oscillations about the steady-state value of $i/i_{LIM}$ corresponding to a light flux of $(J_o + I_o)/2$, the average value of $I(t)$, are observed. The analysis of Fig. 7 illustrates that the variation of the light-source cycle period can be used as valuable tool in the analysis of PEC systems.

The effect of varying the degree of reverse bias is portrayed in Fig. 8. In this work, we have assumed that the space-charge region is in a state of equilibrium, and may be mathematically described by Eq. 11. Consequently, if all of the light absorption were to take place within the space-charge region, a pseudosteady-state expression would describe the current-time relationship. This predicted behavior is shown in Fig. 8. For a large space-charge width $w$, corresponding to a large reverse bias (a large value of $a\lambda_D\sqrt{z_o f(V - V_{FB})}$, displayed with the dashed curve in Fig. 8) the current response is nearly in phase with the sinusoidal light flux. For this case, the light flux could be substituted into Eq. 56 to obtain a similar current

response. The solid curve in Fig. 8, corresponding to a narrower space-charge region, has a significant phase lag relative to the dashed curve. An experimenter can control the thickness of the space-charge region by varying the potential of the working electrode and obtain different current responses that can be described by the equations presented in this work.

## Conclusion

Analytic solutions have been obtained for the minority-carrier concentration at a semiconductor surface during pulse (Eq. 37), step (Eq. 41), sinusoidal and periodic square-pulse (Eq. 52) illumination of a semiconductor-electrolyte interface. The analytic solutions can serve as useful comparisons for more general modeling of the unsteady-state illumination of a semiconductor-electrolyte interface. In addition, the analytic solutions can be used to describe accurately the low-level-injection behavior of wide-band-gap semiconductors commonly used in photoelectrolysis cells and other photoelectrochemical systems. For these systems, since the periodic illumination of a photoelectrochemical cell results in a periodic photoresponse, the analytic solutions are useful for the evaluation of system physicochemical parameters. The periodic-illumination technique is analogous to the traditional cyclic chronopotentiometry and chronoamperometry electrochemical techniques. In particular, the cycle period of the varying light source can be adjusted to match the time constants of the photoelectrochemical cell processes, which makes this technique a valuable analytical tool for the investigation of semiconductor-electrolyte interfaces.

## Acknowledgment

This work was supported by the Director, Office of Energy Research, Office of Basic Energy Sciences, Materials Sciences Division of the Office of the U.S. Department of Energy, under contract no. DE-AC03-76SF00098.

## LIST OF SYMBOLS

| | |
|---|---|
| $a$ | light-absorption coefficient, 1/cm |
| $c$ | concentration, mol/cm$^3$ |
| $D$ | diffusion coefficient, cm$^2$/s |
| $e^-$ | symbol for the electron |
| $E$ | measured electrode potential, V |
| $f$ | $F/(RT)$, 1/V |
| $F$ | Faraday's constant, C/equivalent |
| $i$ | current density, A/cm$^2$ |
| $I$ | incident light flux, mol/(cm$^2$ – s) |
| $k_a$, $k_c$ | anodic and cathodic rate constants, kg/(cm$^2$ – s) |
| $L$ | diffusion length, cm |
| $\mathcal{L}^{-1}$ | symbol for the inverse Laplace transform |
| $n$ | number of electrons in a reaction |
| $R$ | universal gas constant, 8.314 J/mol-K |
| $s$ | Laplace transform variable, 1/s |
| $s_i$ | stoichiometric coefficient of species $i$ |
| $t$ | time, s |
| $T$ | absolute temperature, K |
| $T_c$ | one half the cycle period, s |
| $U^\circ$ | standard electrode potential, V |
| $v_s$ | surface-recombination velocity, cm/s |
| $V$ | electrode potential defined by Eq. 3, V |
| $V_{FB}$ | flat-band potential, V |
| $w$ | space-charge thickness, cm |
| $x$ | distance variable, cm |
| $z_i$ | charge number of species $i$ |
| $z_o$ | charge number of the major semiconductor-dopant atoms |

Greek characters

| | |
|---|---|
| $\alpha$ | dimensionless light-absorption coefficient |
| $\beta$ | symmetry factor |
| $\varsigma$ | dimensionless distance variable |
| $\theta$ | dimensionless time |
| $\Theta$ | dimensionless concentration |
| $\lambda$ | dimensionless current density |
| $\lambda_D$ | Debye length, cm |
| $\mu_i$ | electrochemical potential of species $i$ |

| | |
|---|---|
| $\rho_o$ | solvent density, kg/cm$^3$ |
| $\sigma_1$ | dimensionless constant defined in Eq. 34 |
| $\sigma_2$ | dimensionless group defined in Eq. 35 |
| $\tau$ | carrier lifetime, s |
| $\phi$ | dimensionless incident light flux |
| $\Phi$ | electrical potential, V |

Subscripts

| | |
|---|---|
| $IR$ | ohmic |
| $MS$ | metal-semiconductor interface |
| $SE$ | semiconductor-electrolyte interface |
| $ref$ | reference electrode compartment |

Superscripts

| | |
|---|---|
| $b, s$ | bulk semiconductor |
| $eq$ | equilibrium |
| $init$ | initial |
| $o, Pt$ | reference state in the platinum phase |
| $o, s$ | reference state in the semiconductor phase |
| $surf$ | surface |
| $\theta$ | reference state in the aqueous phase |

## REFERENCES


1. W.H. Brattain and C.G.B. Garett, *Bell Syst. Tech. J.*, 34(1955)129.
2. H. Reiss, *J. Electrochem. Soc.*, 125(1978)937.
3. A.J. Bard, *J. Electroanal. Chem.*, 168(1984)5.
4. A. Heller, *Science*, 223(1984)1141.
5. R.G. Shulman, *Semiconductors*, N.B. Hannay, editor, Reinhold, New York, 1959, pp. 493-496.
6. R.H. Bube, *Photoconductivity of Solids*, John Wiley and Sons, New York, 1960, p. 425.
7. G.M. Martin and D. Bois, *Semiconductor Characterization Techniques*, P.A. Barnes and G.A. Rozgonyi, editors, The Electrochemical Society, New York, 1978, pp. 32-42.
8. W.W. Gartner, *Phys. Rev.*, 116(1959)84.
9. J.F. Dewald, *Semiconductors*, N.B. Hannay, editor, Reinhold, New York, 1959, pp. 737-739.
10. Y.G. Chai and W.W. Anderson, *J. Appl. Phys.*, 27(1975)183.
11. M.A. Butler, *J. Appl. Phys.*, 48(1977)1914.
12. W. Kautek, H. Gerisher, and H. Tributsch, *J. Electrochem. Soc.*, 127(1980)2471.
13. W.L. Ahlgren, *J. Electrochem. Soc.*, 128(1981)2123.
14. P. Lemasson, A. Etcheberry, and J. Gautron, *Electrochim. Acta.*, 27(1982)607.
15. W. van Roosbroeck, *J. Appl. Phys.*, 26(1955)380.
16. G.C. Barker, A.W. Gardner, and D.C. Sammon, *J. Electrochem. Soc.*, 113(1966)1182.
17. J. O'M. Bockris and K. Uosaki, *ibid.*, 124(1977)1348.
18. F. Decker and M. Fracastoro-Decker, *J. Electroanal. Chem.*, 126(1981)241.
19. S. Gottesfeld and S.W. Feldberg, *ibid.*, 146(1983)47.
20. L.M. Peter, J. Li, and R. Peat, *ibid.*, 165(1984)29.

21. D. Laser and A.J. Bard, *J. Electrochem. Soc.*, 123(1976)1828, 1833, and 1837.

22. H. Gerisher, *J. Electroanal. Chem.*, 58(1975)263.

23. H. Gerisher, *Physical Chemistry, an Advanced Treatise*, volume IXA, H. Eyring, editor, Academic Press, New York, 1970, pp. 463-542.

24. J. O'M. Bockris and S.U.M. Khan, *J. Electrochem. Soc.*, 132(1985)2648.

25. M.E. Orazem and J. Newman, *J. Electrochem. Soc.*, 131(1984)2569, 2574, and 2582.

26. A.J. Bard and L.R. Faulkner, *Electrochemical Methods*, John Wiley and Sons, New York, 1980, p. 60.

27. M.E. Orazem and J. Newman, *J. Electrochem. Soc.*, 131(1984)2715.

28. T.B. Grimley, *Proc. Roy. Soc. London, ser. A*, 201(1950)40.

29. M. Green, *Modern Aspects of Electrochemistry*, volume 2, J. O'M Bockris, editor, Academic Press, 1959, pp. 370-372.

30. *Ohmic Contacts to Semiconductors*, Bertram Schwartz, editor, The Electrochemistry Society, New York, 1968.

31. J. Newman, *Electrochemical Systems*, Prentice-Hall, Englewood Cliffs, New Jersey, 1973.

32. W. Shockley and W.T. Read, *Phys. Rev.*, 87(1952)835.

33. R.N. Hall, *ibid.*, 87(1952)387.

34. A.S. Grove, *Physics and Technology of Semiconductor Devices*, John Wiley and Sons, New York, 1967, pp. 183-186.

35. R.S. Muller and T.I. Kamis, *Device Electronics for Integrated Circuits*, John Wiley and Sons, New York, 1977, pp. 165-179.

36. S.M. Sze, *Semiconductor Devices, Physics and Technology*, John Wiley and Sons, New York, 1985, pp. 87-92.

37. F.B. Hildebrand, *Advanced Calculus for Applications*, second edition, Prentice-Hall, Englewood Cliffs, New Jersey, 1976.

38. *Handbook of Mathematical Functions*, M. Abramowitz and I.A. Stegun, editors, Dover Publications, New York, 1972.

39. G.E. Roberts, *Table of Laplace Transforms*, W.B. Saunders Company, Philadelphia, Pennsylvania, 1966.

40. F. Oberhettinger and L. Badii, *Tables of Laplace Transforms*, Springer-Verlag, New York, 1973.

41. *Standard Math Tables*, S.M. Selby, editor, CRC Press, Cleveland, Ohio, 1972, p. 480.

42. I.S. Gradshteyn and I.M. Rhzhik, *Tables of Integrals, Series, and Products*, fourth edition prepared by Yu. V. Geronimus and M. Yu. Tseytlin, translation editor A. Jeffrey, Academic Press, New York, 1965, p. 484.

## Appendix

### *Inversion of Equation 40*

The only inversion needed to obtain Eq. 40 from Eq. 39 that is not tabulated is presented below. Using the convolution theorem (ref. 37, p.63), we can write the following:

$$\begin{aligned} \mathcal{L}_I^{-1} &= \mathcal{L}^{-1}\left[\frac{\sqrt{s+1}}{s(s+1-\alpha^2)}\right] \\ &= \int_0^\theta \mathcal{L}^{-1}\left(\frac{1}{s}\right)\Big|_{\theta-\tilde{\theta}} \mathcal{L}^{-1}\left[\frac{\sqrt{s+1}}{(s+1-\alpha^2)}\right]\Big|_{\tilde{\theta}} d\tilde{\theta} \end{aligned} \tag{58}$$

The translation property allows for the evaluation of the product of the inversions within the integral:

$$\mathcal{L}_I^{-1} = \int_0^\theta \frac{e^{-\tilde{\theta}}}{\sqrt{\pi\tilde{\theta}}} d\tilde{\theta} + \int_0^\theta a e^{(\alpha^2-1)\tilde{\theta}} \mathrm{erf}(\alpha\sqrt{\tilde{\theta}}) d\tilde{\theta} \tag{59}$$

The first integral is $\mathrm{erf}(\sqrt{\theta})$. The second integral can be evaluated by the *integration by parts* technique. The final answer is

$$\mathcal{L}_I^{-1} = \frac{1}{\alpha^2-1}\left[-\mathrm{erf}(\sqrt{\theta}) + \alpha \mathrm{erf}(\alpha\sqrt{\theta}) e^{(\alpha^2-1)\theta}\right]. \tag{60}$$

### *Inversion of Equation 45*

To invert Eq. 45, *partial fraction expansion* is used:

$$\begin{aligned} \mathcal{L}_{II}^{-1} &= \mathcal{L}^{-1}\left[\frac{\alpha}{(s^2+\gamma_i^2)(s+1-\alpha^2)}\right] \\ &= \mathcal{L}^{-1}\left\{\frac{\alpha}{(1-\alpha^2)^2+\gamma_i{}^2}\left[\frac{1-\alpha^2-s}{(s^2+\gamma_i{}^2)} + \frac{1}{(s+1-\alpha^2)}\right]\right\} \end{aligned} \tag{61}$$

In the expanded form, the inversion of $\mathcal{L}_{II}^{-1}$ can be evaluated to yield

$$\mathcal{L}_{II}^{-1} = \frac{\alpha}{(1-\alpha^2)^2+\gamma_i{}^2}\left[\frac{(1-\alpha^2)}{\gamma_i}\sin(\gamma_i\theta) - \cos(\gamma_i\theta) + e^{(\alpha^2-1)\theta}\right]. \tag{62}$$

The remaining term that requires inversion in Eq. 45 is

$$\mathcal{L}_{III}^{-1} = \mathcal{L}^{-1}\left[\frac{\sqrt{s+1}}{(s^2+\gamma_i^2)(s+1-\alpha^2)}\right] \tag{63}$$

Using the convolution theorem, $\mathcal{L}_{III}^{-1}$ can be expressed as

$$\mathcal{L}_{III}^{-1} = \int_0^\theta \mathcal{L}^{-1}\left[\frac{\sqrt{s+1}}{(s+1-\alpha^2)}\right]\Big|_{\tilde{\theta}} \mathcal{L}^{-1}\left[\frac{1}{(s^2+\gamma_i^2)}\right]\Big|_{\theta-\tilde{\theta}} d\tilde{\theta}. \tag{64}$$

The inversion of the first factor in Eq. 64 was completed in the development of Eq. 59. The inversion of the second bracketed term in Eq. 64 is $\frac{1}{\gamma_i}\sin\left[\gamma_i(\theta-\tilde{\theta})\right]$, which can be expanded in order to express $\mathcal{L}_{III}^{-1}$ as

$$\mathcal{L}_{III}^{-1} = \frac{-1}{\gamma_i}\left[\Xi_1\cos(\gamma_i\theta) - \Xi_2\sin(\gamma_i\theta)\right] - \frac{\alpha}{\gamma_i}\left[\Xi_3\cos(\gamma_i\theta) - \Xi_4\sin(\gamma_i\theta)\right]. \tag{65}$$

where:

$$\Xi_1 = \int_0^\theta \sin(\gamma_i\tilde{\theta})\frac{e^{-\tilde{\theta}}}{\sqrt{\pi\tilde{\theta}}}d\tilde{\theta} \tag{66}$$

$$\Xi_2 = \int_0^\theta \cos(\gamma_i\tilde{\theta})\frac{e^{-\tilde{\theta}}}{\sqrt{\pi\tilde{\theta}}}d\tilde{\theta} \tag{67}$$

$$\Xi_3 = \int_0^\theta \sin(\gamma_i\tilde{\theta})e^{(\alpha^2-1)\tilde{\theta}}\mathrm{erf}(\alpha\sqrt{\tilde{\theta}})d\tilde{\theta} \tag{68}$$

$$\Xi_4 = \int_0^\theta \cos(\gamma_i\tilde{\theta})e^{(\alpha^2-1)\tilde{\theta}}\mathrm{erf}(\alpha\sqrt{\tilde{\theta}})d\tilde{\theta} \tag{69}$$

The functions $\Xi_3$ and $\Xi_4$ can be integrated by making use of the *integration by parts* technique. The task is somewhat arduous, and we will only outline the treatment of $\Xi_3$. The function $\Xi_4$ can be dealt with in an analogous fashion.

To integrate $\Xi_3$ by parts, define

$$u = \sin(\gamma_i\tilde{\theta})\mathrm{erf}(\alpha\sqrt{\tilde{\theta}}), \text{ then} \tag{70}$$

$$du = \left[\gamma_i\cos(\gamma_i\tilde{\theta})\mathrm{erf}(\alpha\sqrt{\tilde{\theta}}) + \sin(\gamma_i\tilde{\theta})\frac{\alpha}{\sqrt{\pi\tilde{\theta}}}e^{\alpha^2\tilde{\theta}}\right]d\tilde{\theta}. \tag{71}$$

Also define

$$dv = e^{(\alpha^2-1)\tilde{\theta}}d\tilde{\theta}, \text{then} \tag{72}$$

$$v = \frac{e^{(\alpha^2-1)\tilde{\theta}}}{\alpha^2-1}. \tag{73}$$

$\Xi_3$ can be then be written as $\Xi_3 = uv - \int v du\Big|_0^\theta$, or

$$\Xi_3 = \frac{e^{(\alpha^2-1)\tilde{\theta}}}{\alpha^2-1}\sin(\gamma_i\tilde{\theta})\mathrm{erf}(\alpha\sqrt{\tilde{\theta}}) - \frac{\alpha^2}{\alpha^2-1}\Xi_1 - \frac{\gamma_i}{\alpha^2-1}\int \cos(\gamma_i\tilde{\theta})\mathrm{erf}(\alpha\sqrt{\tilde{\theta}})e^{(\alpha^2-1)\tilde{\theta}}d\tilde{\theta}\Big|_0^\theta. \tag{74}$$

The last term in Eq. 74 can be integrated by parts again. For this integration, $\sin(\gamma_i\tilde{\theta})$ in Eq. 70 is replaced with $\cos(\gamma_i\tilde{\theta})$, and Eq. 72 is used again for the definition of $v$. Performing the integration, Eq. 74 becomes

$$\Xi_3 = \frac{e^{(\alpha^2-1)\tilde{\theta}}}{\alpha^2-1}\sin(\gamma_i\tilde{\theta})\mathrm{erf}(\alpha\sqrt{\tilde{\theta}}) - \frac{\alpha}{\alpha^2-1}\Xi_1 - \frac{\gamma_i}{\alpha^2-1}\left[\frac{e^{(\alpha^2-1)\tilde{\theta}}}{\alpha^2-1}\cos(\gamma_i\tilde{\theta})\mathrm{erf}(\alpha\sqrt{\tilde{\theta}}) + \frac{\gamma_i}{\alpha^2-1}\Xi_3 - \frac{\alpha}{\alpha^2-1}\Xi_2\right]\Bigg|_0^{\theta}. \tag{75}$$

Equation 75 can be solved algebraically for $\Xi_3$. The resulting expressions for $\Xi_3$ and the function $\Xi_4$ are:

$$\Xi_3 = \frac{1}{1+\frac{\gamma_i^2}{(\alpha^2-1)^2}} \times \left[\frac{e^{(\alpha^2-1)\theta}}{\alpha^2-1}\sin(\gamma_i\theta)\mathrm{erf}(\alpha\sqrt{\theta}) - \frac{\gamma_i}{(\alpha^2-1)^2}e^{(\alpha^2-1)\theta}\cos(\gamma_i\theta)\mathrm{erf}(\alpha\sqrt{\theta}) - \frac{\alpha}{\alpha^2-1}\Xi_1 + \frac{\alpha\gamma_i}{(\alpha^2-1)^2}\Xi_2\right], \tag{76}$$

and

$$\Xi_4 = \frac{1}{1+\frac{\gamma_i^2}{(\alpha^2-1)^2}} \times \left[\frac{e^{(\alpha^2-1)\theta}}{\alpha^2-1}\cos(\gamma_i\theta)\mathrm{erf}(\alpha\sqrt{\theta}) - \frac{\gamma_i}{(\alpha^2-1)^2}e^{(\alpha^2-1)\theta}\sin(\gamma_i\theta)\mathrm{erf}(\alpha\sqrt{\theta}) - \frac{\alpha}{\alpha^2-1}\Xi_2 - \frac{\alpha\gamma_i}{(\alpha^2-1)^2}\Xi_1\right]. \tag{77}$$

The functions $\Xi_3$ and $\Xi_4$ can be placed into Eq. 65 to yield $\mathcal{L}_{III}^{-1}$. $\mathcal{L}_{II}^{-1}$ and $\mathcal{L}_{III}^{-1}$ (Eqs. 61 and 65, respectively) can then be combined with Eq. 45 to obtain $\frac{d\Theta}{d\varsigma}\Big|_{\varsigma=0}$.

A straightforward integration of $\Xi_1$ and $\Xi_2$ does not appear possible. The integrands of these functions, however, can be expressed in a power series, which can be integrated to yield the expressions given in Eqs. 48 and 49. For long times, the integral expressions for $\Xi_1$ and $\Xi_2$, Eqs. 66 and 67, reach limiting values listed in Eqs. 50 and 51 (42).

## Figure Captions

Fig. 1. Schematic illustration of a semiconductor-electrolyte interface.

Fig. 2. Impulse light-flux function.

Fig. 3. Step light-flux function.

Fig. 4. Sinusoidal and periodic-square-pulse light-flux functions.

Fig. 5. Current-density response to an impulse light-flux function. For this plot, $a\lambda_D\sqrt{z_o f(V - V_{FB})} = 0.010$.

Fig. 6. Current-density response to a light-step function. For this plot, $a\lambda_D\sqrt{z_o f(V - V_{FB})} = 0.010$.

Fig. 7. Current-density response to a sinusoidal light source. The ratio of the light-source cycle period to the minority-carrier lifetime is listed. For this plot, $a\lambda_D\sqrt{z_o f(V - V_{FB})} = 1.00 \times 10^{-5}$.

Fig. 8. Current-density response to a sinusoidal light source. The dimensionless potential $a\lambda_D\sqrt{z_o f(V - V_{FB})}$ is given. $(T_c/\tau = 0.010)$

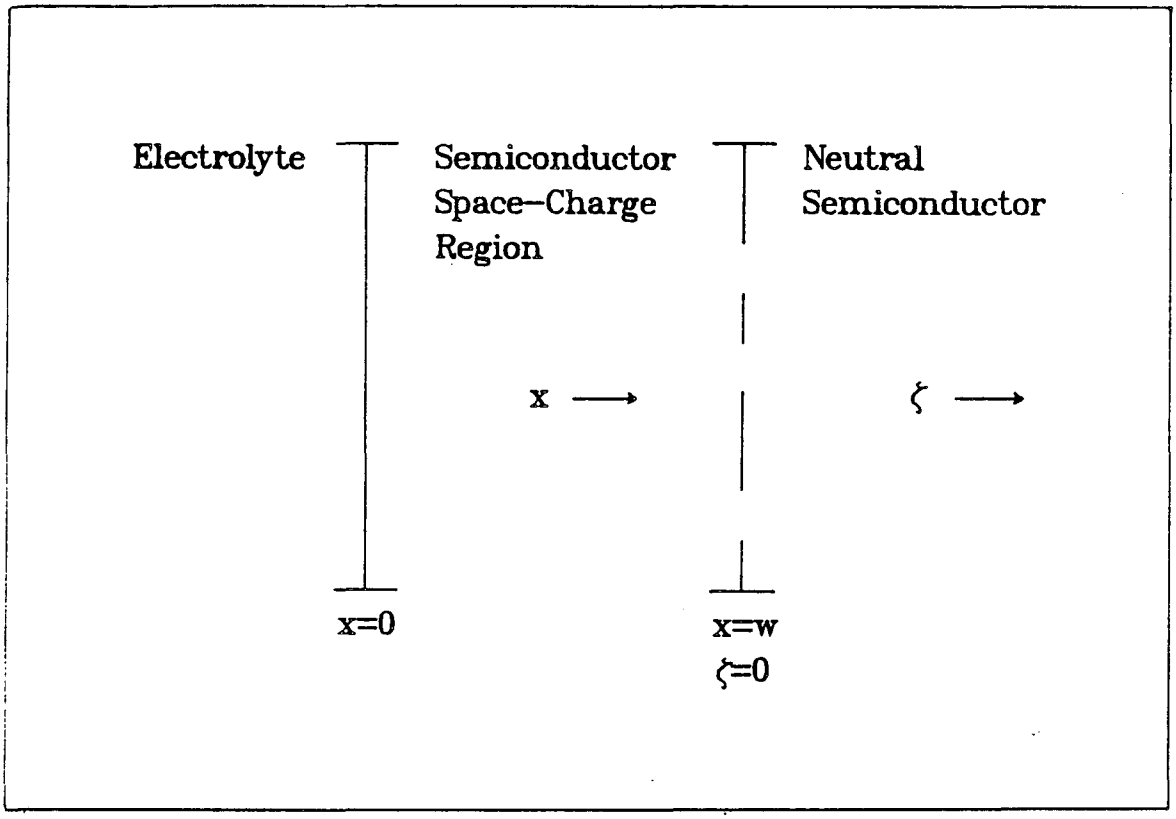
Electrolyte
Semiconductor
Space–Charge
Region
Neutral
Semiconductor
x
ζ
x=0
x=w
ζ=0

FIGURE 1

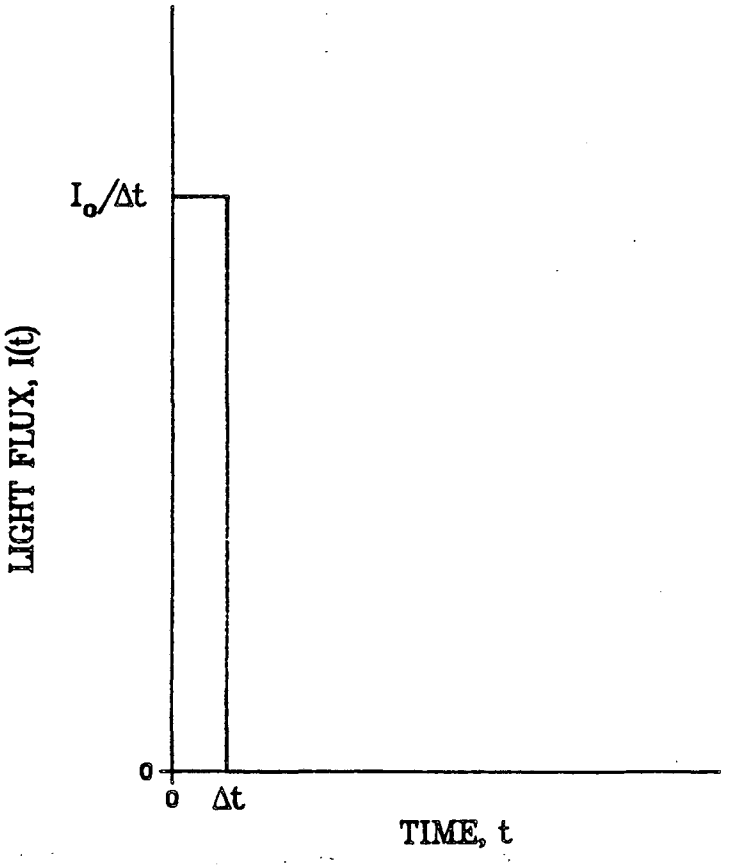


FIGURE 2

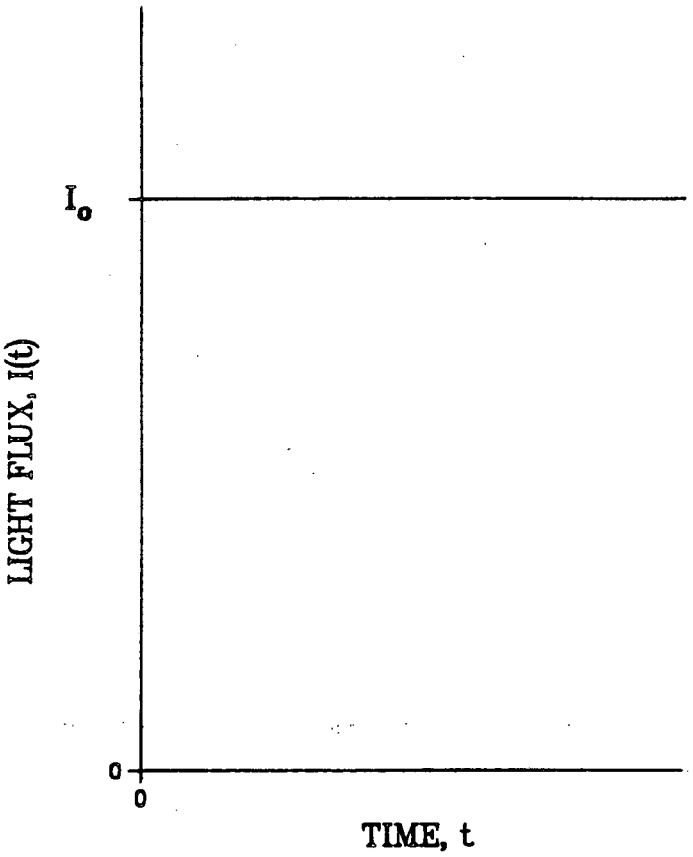


FIGURE 3

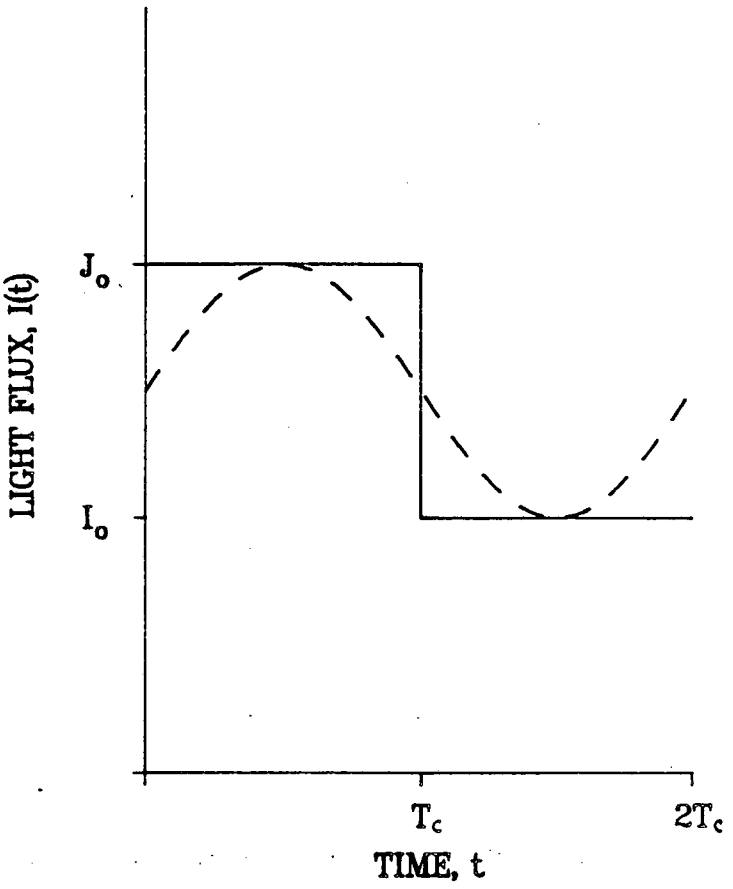


FIGURE 4

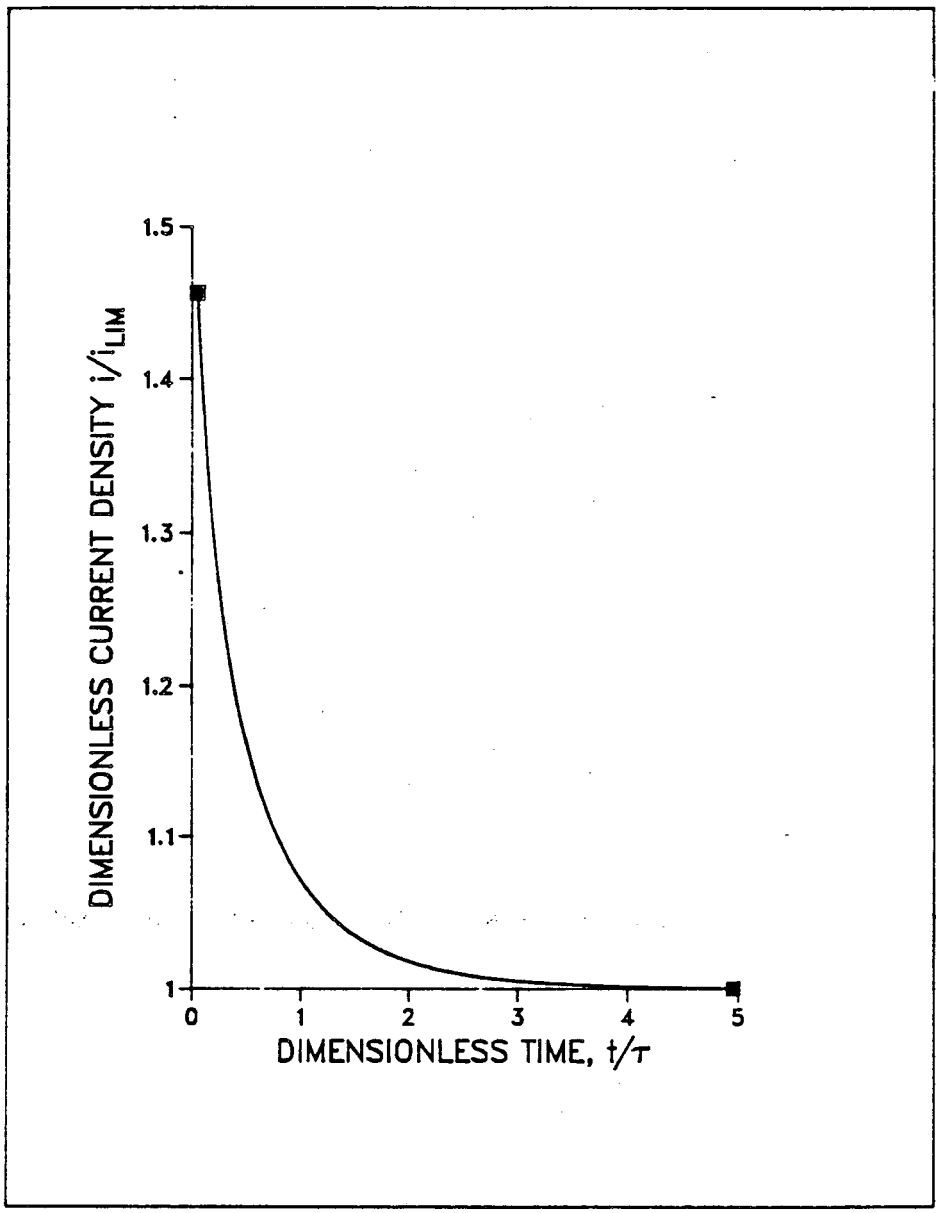
DIMENSIONLESS CURRENT DENSITY $i/i_{LIM}$
1.5
1.4
1.3
1.2
1.1
1
0
1
2
3
4
5
DIMENSIONLESS TIME, $t/\tau$

FIGURE 5

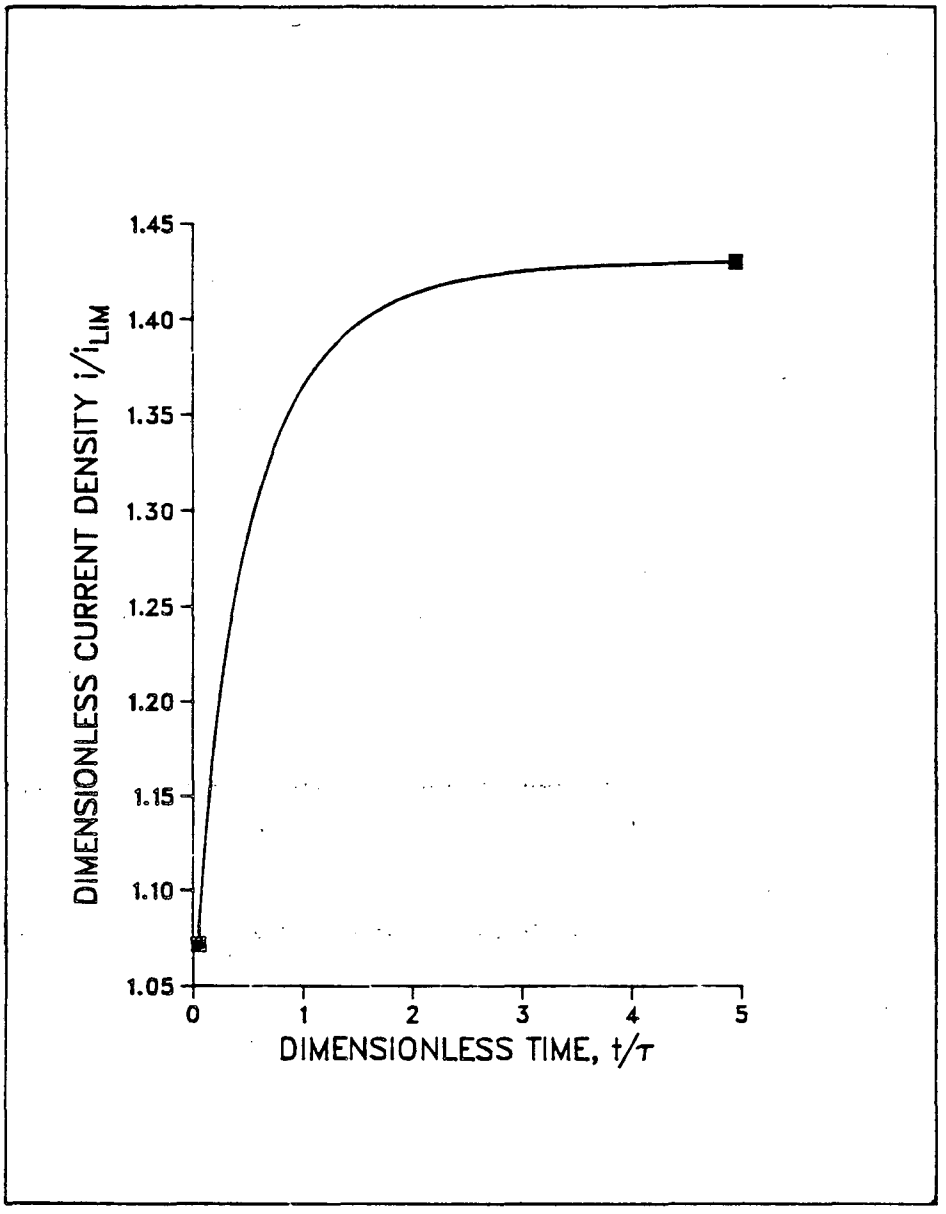
DIMENSIONLESS CURRENT DENSITY $i/i_{LIM}$
1.45
1.40
1.35
1.30
1.25
1.20
1.15
1.10
1.05
0
1
2
3
4
5
DIMENSIONLESS TIME, $t/\tau$

FIGURE 6

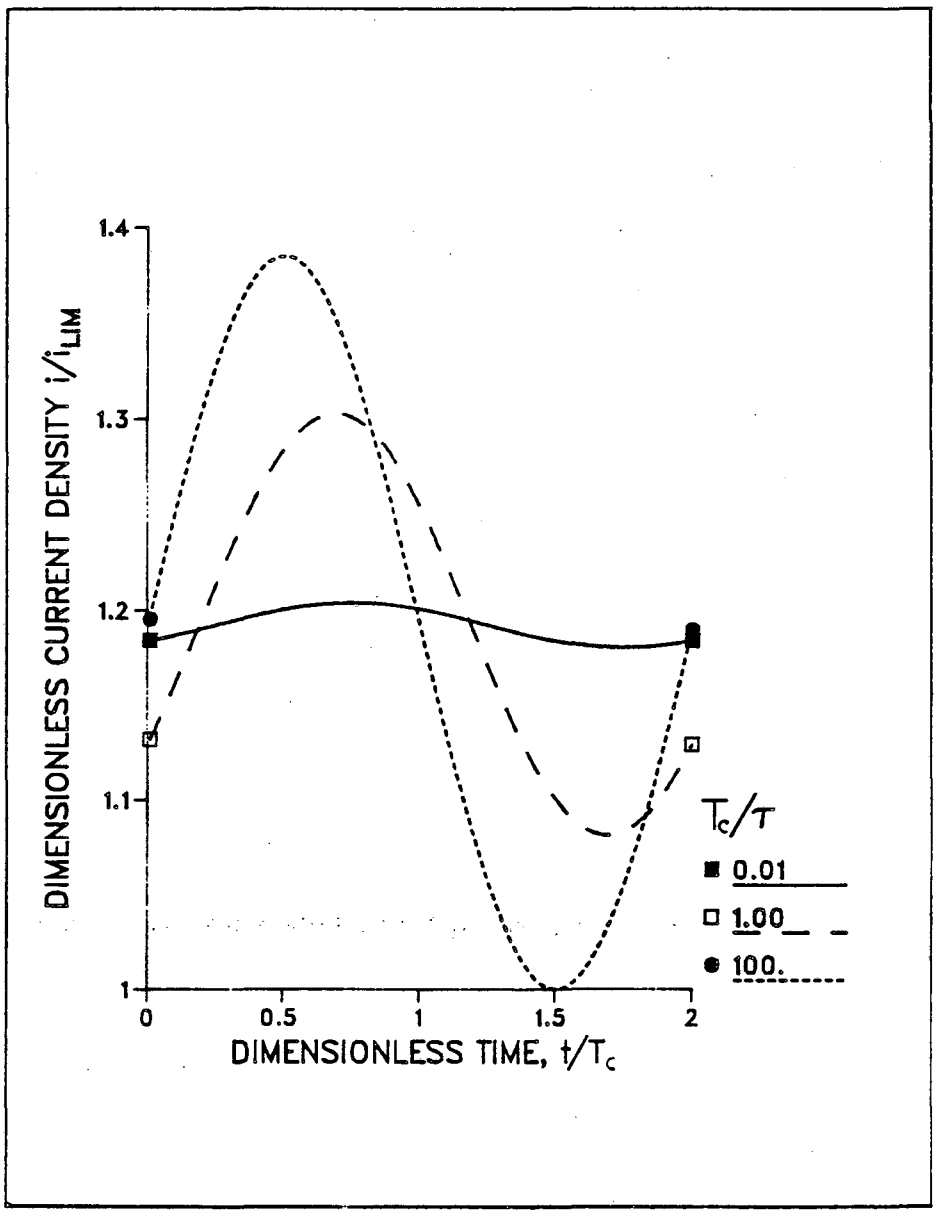
DIMENSIONLESS CURRENT DENSITY $i/i_{LIM}$
1.4
1.3
1.2
1.1
1
0
0.5
1
1.5
2
DIMENSIONLESS TIME, $t/T_c$
$T_c/T$
0.01
1.00
100.

FIGURE 7

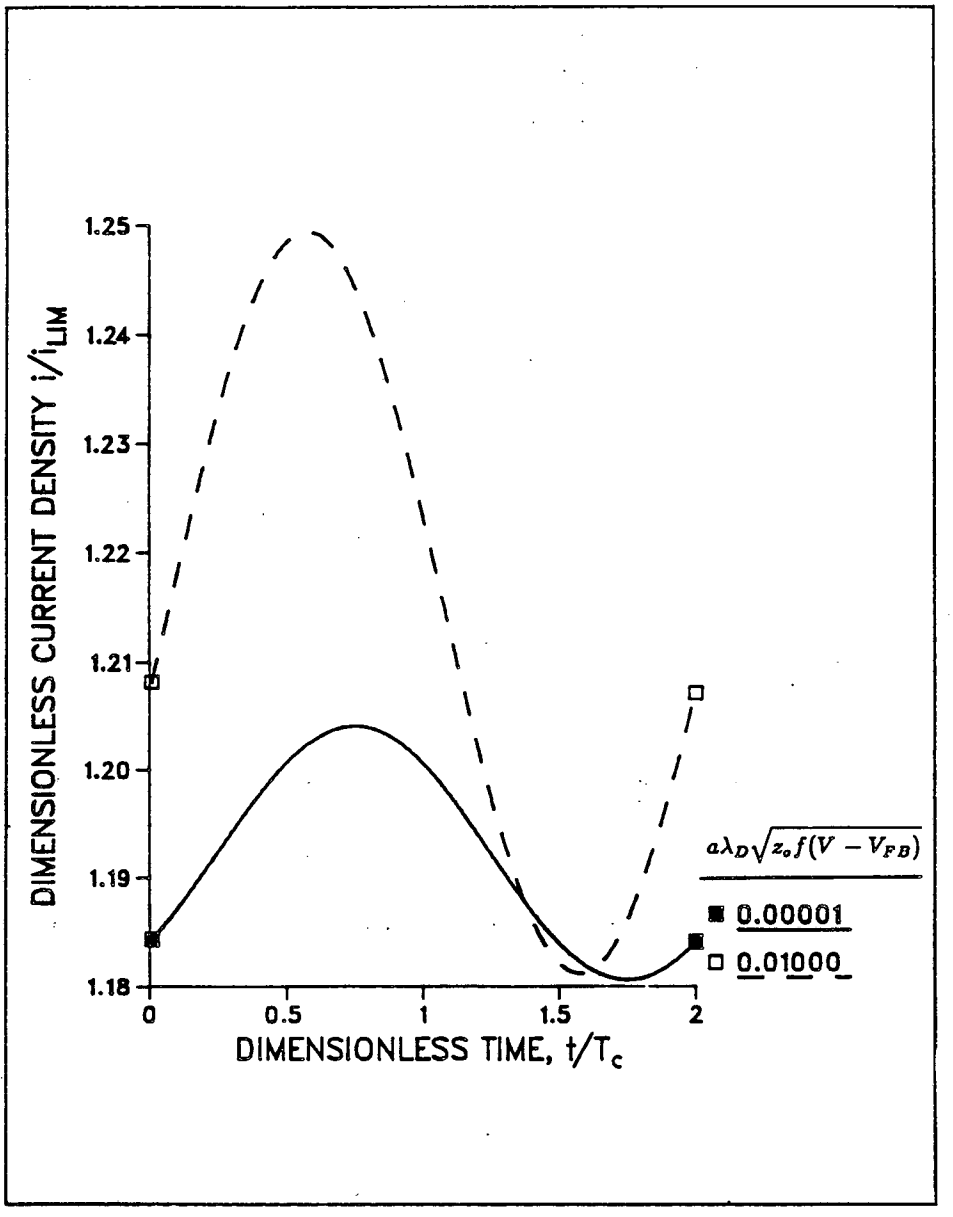
DIMENSIONLESS CURRENT DENSITY $i/i_{LIM}$
1.25
1.24
1.23
1.22
1.21
1.20
1.19
1.18
0
0.5
1
1.5
2
DIMENSIONLESS TIME, $t/T_c$
$a\lambda_D\sqrt{z_o f(V - V_{FB})}$
0.00001
0.01000

FIGURE 8

This report was done with support from the Department of Energy. Any conclusions or opinions expressed in this report represent solely those of the author(s) and not necessarily those of The Regents of the University of California, the Lawrence Berkeley Laboratory or the Department of Energy.

Reference to a company or product name does not imply approval or recommendation of the product by the University of California or the U.S. Department of Energy to the exclusion of others that may be suitable.

*LAWRENCE BERKELEY LABORATORY*
*TECHNICAL INFORMATION DEPARTMENT*
*UNIVERSITY OF CALIFORNIA*
*BERKELEY, CALIFORNIA 94720*